



## Enhancement of Heavy Vacuum Gas Oil Desulfurization Via Using Developed Catalyst Based on Al<sub>2</sub>O<sub>3</sub>



Asmaa, I. Zahran <sup>\*1</sup>, Ahmed M.A. El Naggar <sup>1</sup>, Wael A. Aboutaleb <sup>1</sup>,  
Mohamed A. Sayed <sup>1</sup>, Huda, S. Ahmed <sup>1</sup>, Mohamed A. Mekewi <sup>2</sup>

1. Egyptian Petroleum Research Institute, 1A Ahmed El-Zomor st. Naser city, Cairo
2. Faculty of science, Chemistry dept., Ain-Sham, University, Cairo, Egypt

### Abstract

In past few decades, a strong attention is paid to develop high-active catalysts for hydrotreating of the heavy vacuum gas oil (HVGO). In an agreement with that claim, this research work reports the synthesis of a developed catalyst for desulfurization of a petroleum HVGO fraction. Particularly, the catalytic performance of the catalyst, which was made via addition of CeO<sub>2</sub> to  $\gamma$  alumina as supports for a trimetallic composite (CoNiMo-Al<sub>2</sub>O<sub>3</sub>), toward sulfur removal was investigated. For proper comparison, the activity of alumina individually supported trimetallic catalyst CoNiMo- $\gamma$ Al<sub>2</sub>O<sub>3</sub> at such application was also studied. The as-prepared catalysts were characterized by X-ray diffraction (XRD), transmission electron microscopy (TEM) and N<sub>2</sub> physical adsorption/desorption (BET). Catalytic activity was conducted in continuous flow trickle-bed reactor at various operating condition of temperature (320-380 °C), pressure (20-60 bar) and liquid hour space velocity (1-2.5 h<sup>-1</sup>). It was found that CoNiMo/CeO<sub>2</sub>- $\gamma$ Al<sub>2</sub>O<sub>3</sub> was of a higher catalytic efficiency to hydrotreating of HVGO than that of CoNiMo-Al<sub>2</sub>O<sub>3</sub>. Numerically, CoNiMo/CeO<sub>2</sub>- $\gamma$ Al<sub>2</sub>O<sub>3</sub> could successfully remove 83.5 % of sulfur compounds while it was only 66.2% in case of CoNiMo-Al<sub>2</sub>O<sub>3</sub>. The increased catalytic performance of ceria containing composite may be due to its high specific surface area (~198.4 m<sup>2</sup>.g<sup>-1</sup>) and small crystallite size (24.24 nm). Moreover, the incorporation of CeO<sub>2</sub> to alumina could subsequently inhibit the interaction between Ni and alumina; hence the inactive NiAl<sub>2</sub>O<sub>4</sub> phase had not been formed. Thus, an enhanced catalytic desulfurization process could be attained

Keywords: Hydrodesulfurization, Vacuum gas oil, Ceria-alumina catalyst, Nickel-cobalt-Molybdenum catalyst, Trickle-bed reactor.

### 1. Introduction

World energy demand is expected to increase over the years, as the growth of population and urbanization persistently increased. Therefore, the demand for clean fuel considers one of the main technical and economic challenges facing the refining industry during over the last years [1, 2]. Heavy vacuum gas oils are characterized as having relatively high specific gravity, low hydrogen-to-carbon ratios, and high

carbon residue, boiling point about (343-550 °C) and contain large amounts of sulfur, nitrogen and metals. Therefore, upgrading of heavy vacuum gas oil to more useful lighter products is indispensable [3]. In order to meet the requirements of the ecological legislation which is set by US Environmental Protection Agency, the amount of sulfur and nitrogen content need to be lowered to provide a clean environment.

\*Corresponding author e-mail: [Asmaazahran88@yahoo.com](mailto:Asmaazahran88@yahoo.com)

Receive Date: 22 February 2020, Revise Date: 02 March 2020, Accept Date: 08 March 2020

DOI: 10.21608/EJCHEM.2020.24452.2457

©2020 National Information and Documentation Center (NIDOC)

Hydrotreating (HDT) is the main catalytic conversion process, which allows the reducing emission of  $\text{SO}_x$  and  $\text{NO}_x$ , which are synthesized by fuel combustion. These emissions can inhibit the performance of the catalysts used in refining processes, as well as the catalysts used in catalytic converters of vehicles [4]. Up to now, the science community still has a strong interest toward the development of highly active hydrotreating catalysts to efficiently perform such reductions. Among the presented catalysts for such purpose, alumina supported Ni-Mo and CoMo are the most traditionally utilized catalysts [5].

Generally, Co-Mo- $\text{Al}_2\text{O}_3$  catalyst is suitable for fractions of low nitrogen contents and favors the direct desulfurization route. On contrary, Ni-Mo- $\text{Al}_2\text{O}_3$  is suitable for high nitrogen content fractions and favors the direct hydrogenation pathway [6]. Trimetallic catalysts were used to increase the flexibility of catalyst and it will favor both direct desulfurization (DDS) and hydrogenation (HYD) route simultaneously in terms of combining the advantages of both Ni-Mo and Co-Mo catalysts.  $\text{CeO}_2$  loading to alumina provides the advantageous combination of alumina high surface area with the  $\text{CeO}_2$  unique properties [7, 8]. Ceria which is an efficient promoter decreases the carbon deposition on the catalyst surface as it has unique redox property leads to a high oxygen storage capacity [9]. Moreover, the small particles size of  $\text{CeO}_2$  increases the  $\text{Ce}^3$  versus  $\text{Ce}^4$  species, therefore more oxygen deficiency that creates more active sites [10]. Furthermore, ceria promotes the noble metals reduction [11], influences the catalyst structural and electronic properties [12] and enhance the Ni dispersion and reactivity and prevents the Ni particles sintering and  $\text{NiAl}_2\text{O}_4$  inactive phase formation [13]. Thus,  $\text{CeO}_2$ - $\text{Al}_2\text{O}_3$  material still achieved an acceptable economic effective catalyst.

In this research work, Co-Ni-Mo supported on  $\text{CeO}_2$ - $\text{Al}_2\text{O}_3$  is introduced as a novel developed catalyst for the hydrotreatment of petroleum heavy vacuum gas oil. Dual promotion effect of adding Co and Ni with Mo, incorporated in a trimetallic structure, is designated to enhance the catalyst activity than the case of their bimetallic catalysts (Co/ Mo and Ni/Mo). Additionally, doping of ceria on alumina prevent the formation of inactive phase of metals aluminates. Thus, enhancement the catalytic activity, which leads to improvement of HVGO quality, will take place.

## Experimental

### 2.1 Feedstock

Heavy vacuum gas oil (HVGO) fraction, which had been used as feedstock in the present investigation, was conducted from Suez Oil Petroleum Company (SOPC). The main characteristics of this feedstock are indicated in **Table (1)**. All the utilized chemical reagents in this research are acquired from Sigma Aldrich-UK.

**Table (1): Properties of heavy vacuum gas oil feedstock.**

Experiment	Result
Density @ 15.56 °C, g/ml	0.8867
Specific gravity	0.8876
Total sulfur content, wt. %	1.66
Total nitrogen, wt. %	2.97
Aniline point @ °F	165.2
Diesel index, %	46.09
Refractive index @ 20	1.4860
Pour point, °C	+9
Flash point, °C	87
Colour	8
<b>Component analysis</b>	
Total saturates, wt. %	63.88
Total aromatics, wt. %	34
Resin, wt. %	2.12

#### 2.2.1 Preparation of alumina and ceria

Alumina was prepared, by the chemical precipitation method. Typically, a calculated amount of aluminium nitrate  $\text{Al}(\text{NO}_3)_3 \cdot 9\text{H}_2\text{O}$ , corresponding to the required amount of  $\text{Al}_2\text{O}_3$ , was dissolved in deionized water and stirred for 10 min to ensure the solution homogeneity. The aluminium nitrate solution was heated up to a temperature of 70 °C.  $\text{NH}_4\text{OH}$  solution was

subsequently used as a precipitating agent through a drop-wise addition under vigorous stirring (550 rpm). Precipitation of aluminium (as hydroxides) was continued via adding  $\text{NH}_4\text{OH}$  solution until at pH range of 8-8.5 was observed. Afterward, the precipitate was digested overnight at room temperature. Then, the obtained precipitate was filtered and consequently washed with deionized water several times. This precipitate was next dried overnight inside an oven at  $100\text{ }^\circ\text{C}$ . The collected powders of aluminium hydroxide, after drying process, was afterward calcined at  $550\text{ }^\circ\text{C}$  for 4 h to gain their corresponding oxide.

### 2.2.2 Preparation of ceria-alumina

$\text{CeO}_2\text{-Al}_2\text{O}_3$  supports with different atomic ratio of  $\text{Ce}/(\text{Ce} + \text{Al}) = 0.50$  was prepared by the homogeneous co-precipitation method. Typically, calculated amounts of  $\text{Ce}(\text{NO}_3)_3 \cdot 9\text{H}_2\text{O}$ , and  $\text{Al}(\text{NO}_3)_3 \cdot 9\text{H}_2\text{O}$  that correspond to the prior-stated  $\text{Ce}/\text{Al}$  ratio were dissolved in deionized water and stirred for a time of 10 min. The produced mixture was then heated up to  $50\text{ }^\circ\text{C}$  and stirred for further 5 min to attain the highest possible homogeneity. Solutions of  $\text{NH}_4\text{OH}$  (precipitating agent) of similar concentration was then drop-wise added to the mixture under vigorous stirring (550 rpm). Consequently, the precipitation vessels were digested at room temperature for nearly 18 h.

The acquired precipitate, from the Mixture, was then filtered and washed with deionized water several times. The ultimately collected powder after wash was next dried in an oven at  $100\text{ }^\circ\text{C}$  for overnight. The dried powder was subsequently forwarded to a calcinations step at  $550\text{ }^\circ\text{C}$  for 4 h.

### 2.2.3 Loading of Co-Ni-Mo oxides

Catalysts of cobalt-nickel-molybdenum oxides supported on alumina and their composites were prepared. These catalysts were labeled as  $\text{CoNiMo}/\text{CeO}_2\text{-Al}_2\text{O}_3$  and  $\text{CoNiMo}/\text{Al}_2\text{O}_3$ . All these catalysts had contained fixed percentages of the metallic sites as follows: 12 %  $\text{MoO}_3$ , 1.5 %  $\text{NiO}$  and 1.5 %  $\text{CoO}$ , by weight. All of these catalysts were prepared by a pore volume impregnation method [14]. Cobalt acetate, ammonium heptamolybdate tetrahydrate and nickel nitrate were used as the precursor for obtain cobalt, molybdenum, and nickel oxides respectively. Before starting the loading of metallic sites, the total pore volumes of supports were determined by incipient wetness impregnation. Specifically, this technique is based on adding distilled water to degassed alumina and ceria-alumina with syringe. The addition of distilled water was continued until the supports had shown sticky appearance. The value ceria-alumina and alumina

were found to be approximately 1 and  $0.5\text{ mL g}^{-1}$  respectively. Promptly, the loading of metallic sites via impregnation method had launched by completion of former stage. The impregnation was carried out in three subsequent steps in order to avoid accumulation of metals oxides particles. Firstly, the needed amount of ammonium heptamolybdate tetrahydrate was dissolved in a predetermined volume of doubly distilled water. A few drops of  $\text{H}_2\text{O}_2$  were then added to obtain a transparent solution. The amount of hydrogen peroxide had been equivalent to the total pore volume of ceria-alumina and  $\gamma$ -alumina, as previously measured. Then, the prepared mixture of Mo-salt and peroxide was added to the synthesized supports.

After impregnation, the formed moist paste was preliminary dried in an oven at  $120\text{ }^\circ\text{C}$  over night. The dried samples were calcined in a muffle furnace (with a heating rate of  $10\text{ }^\circ\text{C min}^{-1}$ ) at  $550\text{ }^\circ\text{C}$  for 4 h. By the accomplishment of loading molybdenum oxide particles to supports, the loading of other two metals oxide had begun. Particularly, the loading of  $\text{NiO}$  had taken place followed by loading  $\text{CoO}$ . The loading of latter two oxides had typically followed same procedures that were utilized for molybdenum oxide particles.

## 2.3 Catalyst Characterization

### 2.3.1 X-ray diffraction

The X-ray diffraction for the prepared catalyst analysis was performed using X'Pert PRO PANalytical apparatus. The patterns were conducted using Cu K $\alpha$  radiation ( $\lambda = 0.1541\text{ nm}$ ). The  $2\theta$  ranges from  $10^\circ$  to  $70^\circ$  at a scanning rate of  $0.05\text{ s}^{-1}$  were used to record the patterns.

### 2.3.2 Transmission electron microscopy (TEM)

The morphological and structural properties for the catalysts were conducted using a JEOL 2010F TEM apparatus) attached to EDX (Oxford X-Max). It offered high-resolution electron imaging up to  $0.143\text{ nm}$  and magnification as high as 1.5 million times. The images were taken at an accelerating voltage of 200 kV. To prepare the samples, it diluted with 5 ml ethanol to make a suspension. The mixture was sonicated for 20 min then a drop of solution was placed on a carbon coated Cu grid. Ethanol was then slowly evaporated from the Cu grid under a glass cover then the sample was examined.

### 2.3.3 Surface area and pore volume

The physico-chemical properties of the prepared catalyst were determined by  $N_2$  adsorption-desorption method at  $-196\text{ }^\circ\text{C}$ . The BET surface area was measured by using Autosorb 1, Quanta chrome instrument. Prior to the measurement, the catalyst was degassed at  $200\text{ }^\circ\text{C}$  for 4 h to remove the adsorbed gases and moisture. Surface area was calculated using the adsorption data up to a relative pressure of 0.1 by BET method.

### 2.4 Catalytic Activity Test

The hydrotreating experiments were conducted under steady state operation in a fixed bed hydrotreating pilot plant operating in down-flow mode. A detailed scheme of this unit is shown in Fig.1. The system consisted of liquid and gas feeding sections, a high-pressure reactor, a heater with temperature controller for precisely controlling the temperature of the catalyst bed, a scrubber for removing the ammonium sulphide from the reaction products, and a high pressure gas-liquid separator. The reactor is the central part of this plant. It is made of a 316 stainless steel tube. The total length and internal and external diameters of the reactor are 500, 19, and 27 mm, respectively. The reactor temperature was maintained at the desired level by using a three-zone electric furnace, which provided an isothermal temperature along the active reactor section.

#### 2.4.1 Catalyst sulfiding

After loading the catalyst, the catalytic bed was in situ sulfided with a sulfiding feed containing a 6 % dimethyldisulfide (DMDS) in heavy gas oil under the following conditions: pressure = 50 bar; a hydrogen-to-oil ratio = 300 L/L; reaction temperature =  $350\text{ }^\circ\text{C}$ ; and liquid hourly space velocity (LHSV) =  $1\text{ h}^{-1}$ . Presulfiding was continued for 12 h under the stated conditions to ensure complete catalyst presulfiding. When the presulfiding was completed, the feedstock was introduced and sulfiding feed was stopped without stopping the hydrogen flow and the conditions for each run were adjusted to the desired operating temperature, pressure, hydrogen flow rate, and LHSV using HVGO as feedstock.

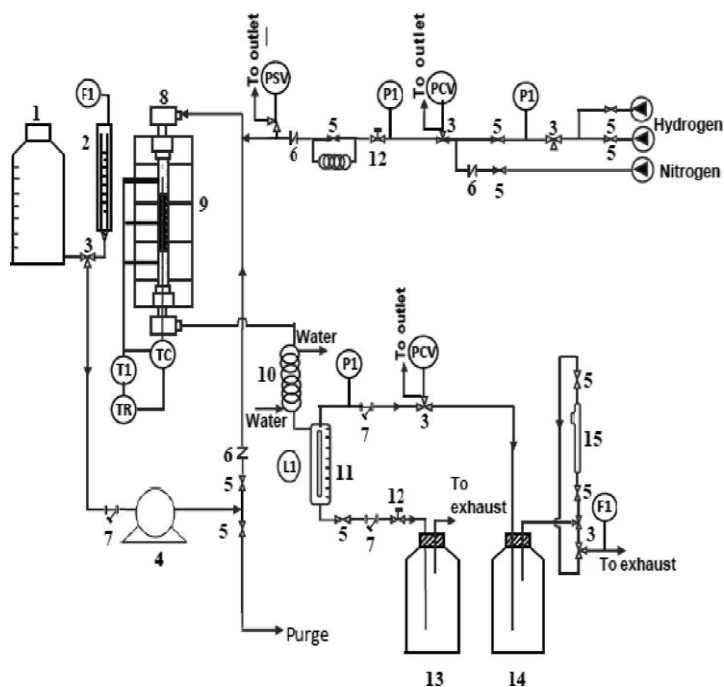


**Fig. 1. Schematic diagram of the HDS reaction system: (PI) pressure indicator; (PCV) pressure cont. valve; (PSV) pressure safety valve; (TI) temperature indicator; (TR) temperature recorder; (TC) level temperature control; (FI) flow indicator; (Li) level indicator; (1) calibrated feed tank; (2) feeder burette; (3) three way valve; (4) feed pump; (5) stop cock; (6) non return valve; (7) filter; (8) reactor; (9) 3-shell furnace; (10) water condenser; (11) separator; (12) adjust cock; (13) calibrated receiving tank; (14) nasal tank and (15) gas sample tube [15].**

## 3. Result and Discussion

The structural and textural characteristics of freshly prepared catalysts had been first discussed through this section. Then, their catalytic performance toward sulfur compounds removal from HVGO is presented.

### 3.1 X-ray diffraction

The Powder X-ray diffraction (XRD) of the freshly prepared pure  $\gamma\text{-Al}_2\text{O}_3$  and (15 %) ceria-alumina supports are illustrated in Fig. 2(a and b). The XRD profile of the pure alumina (Fig. 2a) showed a low intense broad peak at  $2\theta = 37.8^\circ$  and peaks of high intensity at  $45.5$  and  $66.9^\circ$  that are corresponding to the (311), (400) and (440) reflections planes of  $\gamma\text{-Al}_2\text{O}_3$  phase (JCPDS card No. 48-367). The observed broad peaks are referring to highly amorphous nature of alumina particles. The effect of incorporating  $\text{CeO}_2$  with  $\text{Al}_2\text{O}_3$  on the structural characteristics of the subsequently acquired composites is illustrated through Fig. 2b. Tiny peaks at  $2\theta$  of  $45.5$  and  $66.9^\circ$ ,

ascribed to  $\gamma$ - $\text{Al}_2\text{O}_3$ , has been detected in the presented diffractograms. The observation of such low intense peaks can be attributed to the addition of  $\text{CeO}_2$  to  $\text{Al}_2\text{O}_3$  which could probably disperse onto the alumina particles covering its surface. Thus, no strong indicative peaks of alumina could be seen. On the other hand, no peaks that are assigned to  $\text{CeO}_2$  could be detected in the exhibited XRD pattern. This notice can be explained by the high level of ceria particles dispersion within the alumina structure. Similarly, the obtained catalysts after loading the tri-metals oxides had exhibited same XRD patterns (Fig. 2c and 2d) as blank supports. The no observation of indicative peaks for Co, Ni and Mo oxides is also due to the penetration of their particles into the support structures.

Fig. 2d showed only peaks that recorded for the original support. However, the peaks intensities, especially at  $37.4^\circ$  and  $45.5^\circ$  which are corresponding to  $\gamma$ - $\text{Al}_2\text{O}_3$  and/or  $\text{NiAl}_2\text{O}_4$  species, has decreased with incorporation of  $\text{Ce}^{4+}$ . This observation could indicate that less  $\text{NiAl}_2\text{O}_4$  formation on  $\text{CeO}_2$ - $\text{Al}_2\text{O}_3$  catalysts than the loaded alumina catalyst had taken place. This can be explained via either a surface ceria layer formation that prevent the Ni- $\text{Al}_2\text{O}_3$  contact or that the ceria loading caused the existence of small  $\text{NiAl}_2\text{O}_4$  crystals which were undetectable by the XRD apparatus.

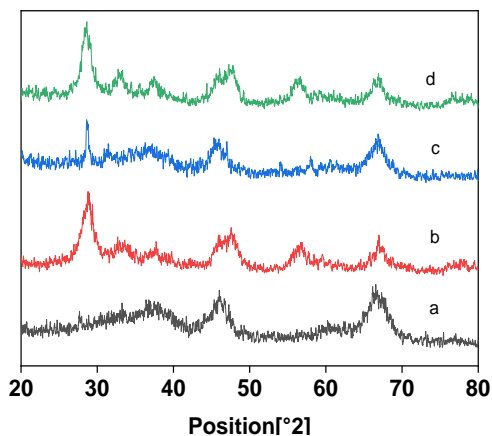


**Fig. 2:** XRD patterns of a) pure alumina, b) 15%  $\text{CeO}_2$ - $\text{Al}_2\text{O}_3$ , c) tri-metals loaded on  $\text{Al}_2\text{O}_3$  and d) metallic sites loaded onto  $\text{CeO}_2$ - $\text{Al}_2\text{O}_3$ .

### 3.2 Transmission Electron Microscopy (TEM)

The morphology of the prepared support (15%  $\text{CeO}_2$ - $\text{Al}_2\text{O}_3$ ) as well as the ultimate catalyst which was obtained after loading of trimetallic sites (on support) is illustrated in Fig. 3. The TEM image of blank  $\text{CeO}_2$ - $\text{Al}_2\text{O}_3$  sample (Fig.3a) showed a flower-like

morphology with a detection of well uniformly distributed  $\text{CeO}_2$  cubic crystalline onto the  $\text{Al}_2\text{O}_3$  surface. High and uniform dispersion of ceria species is most likely referred to the implemented synthesis procedures. Additionally, layered particles of nano-ceria could be also observed at the top part of the given micrograph (Fig 3a). The presence of both ceria and alumina together in the structure had been verified through the displayed EDX spectrum in Fig. 3b. Strong sharp peaks indicative to Ce, Al and oxygen could be noticed. Thus, the production of the prior-stated metals in form of their oxides could be strongly confirmed.

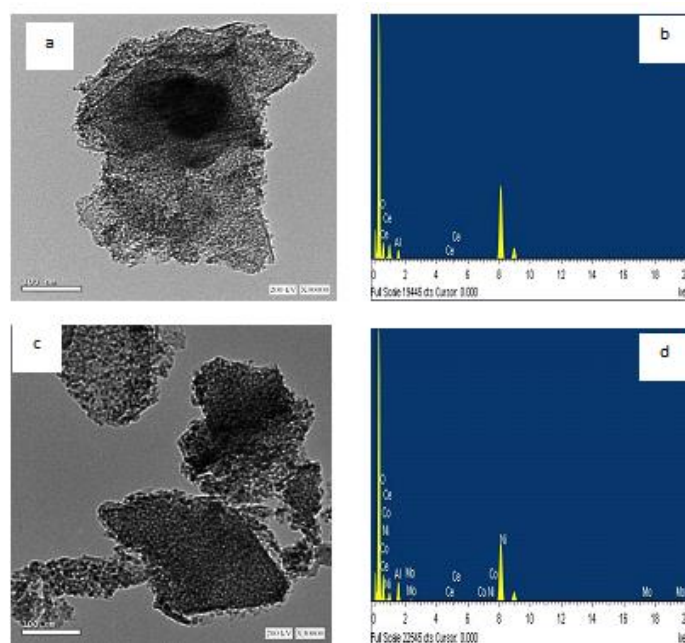


**Fig.3:** Morphological characteristics and elemental analysis of both  $\text{CeO}_2$ - $\text{Al}_2\text{O}_3$  and its sub-driven trimetallic catalyst.

After loading the tri-metallic sites, the produced catalyst had presented uniform appearance. It also had shown similar morphology to that of blank support (Fig. 3c). However, dispersed nanoparticles could be observed onto the support structure. These particles are mainly assigned to the present Mo, Co and Ni oxides in the catalyst composition. The presence of such oxides was verified through the given EDX spectrum in Fig. 3d. In particular, highly intense peak of oxygen and others of proper intensities that belong to Mo, Ni and Co had been noticed.

### 3.3 Surface characteristics

The surface properties of  $\text{Al}_2\text{O}_3$  and 15%  $\text{CeO}_2$ - $\text{Al}_2\text{O}_3$  supports as well as their subsequently generated catalysts are illustrated in Table 2. The data indicated that the 15%  $\text{CeO}_2$ - $\text{Al}_2\text{O}_3$  support showed the higher

## ENHANCEMENT OF HEAVY VACUUM GAS OIL DESULFURIZATION

surface area ( $198.4\text{m}^2/\text{g}$ ) than that the assigned for the  $\text{Al}_2\text{O}_3$ . The increased surface area of Binary support can be referred to the dispersion of ceria particles in between alumina ones. Hence, higher pore volume for ceria-alumina structure could be obtained. Thus, its surface area could be increased over the Pure alumina. BET surface areas after loading the metallic sites on both supports are found to be less compared to that of their blanks. This may be due to the blocking of supports pores by the added Mo, Ni and Co species. Similar trend is observed for the displayed values of pore volume and average pore diameter of catalysts. It indicates that the added Mo, Ni and Co particles entered into the pores of the supports, resulting a significant fall in textural characteristics of the catalysts.

**Table 2: Surface area, pore volume and average pore radius values of the prepared structures.**

Sample	d-XRD	BET surface area ( $\text{m}^2/\text{g}$ )	Total pore volume ( $\text{cm}^3/\text{g}$ )	Average pore diameter (nm)
$\gamma\text{-Al}_2\text{O}_3$	24.9	184.491	0.3	6.7
(15%) $\text{CeO}_2\text{-Al}_2\text{O}_3$	22.8	198.4	0.35	35.6
$\text{CoNiMo/Al}_2\text{O}_3$	56.6	164.531	0.21	5.16
(15%) $\text{CoNiMo/Ce-Al}$	24.2	138.3	0.2	29.7

### 3.4 Catalytic activity

In this stage of current investigation, the effect of different operational conditions on desulfurization rates, by the two prepared catalysts, is discussed. Particularly, relation between changes of temperature, pressure and LHSV and sulfur compounds removal was tracked.

#### 3.4.1 Effect of reaction temperature

The influence of reaction temperature variation on efficiency of the catalysts is illustrated through Fig.4. This step was carried out at a constant pressure of 40 bar and LHSV equals 1. It could be observed that the two catalysts had presented continuous elevation in the percentages of hydrodesulfurization (HDS), hydrodenitrogenation (HDN) and hydrodearomatization (HAD) by the temperature increase. The increased sulfur and nitrogen

compounds removals that were attained at the highest reaction temperature may be attributed to two reasons. First one is that the increase of temperature could result in properly activating the un-reactive sulfur and nitrogen compounds to become able to react with hydrogen due to the increase of their activation energy. Secondly, the sulfur and nitrogen containing molecules could decompose to smaller molecules. Therefore, they can easily diffuse into the micro and meso-pores of the introduced catalyst and reach its inner active sites where the desulfurization reaction mainly occurs [16, 17].

However, remarkable increases in the values of sulfur, nitrogen and aromatics compounds removal by the increase of temperature from 320 to 360 °C could be generally noticed for both catalysts. The subsequent increase of reaction temperature to 380 °C had attained slight increases in the percentages of HDS, HDN and HDA. They showed respective increases of 2, 0.4 and less than 4 Wt. % at the highest operational temperature. Therefore, the operating temperature of 360 °C had been selected as the optimum to be introduced in the next step of the current investigation.

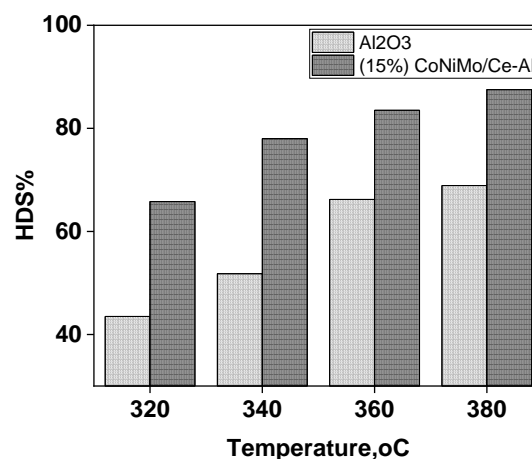


**Fig. 4a: Effect of reaction temperature on hydrodesulfurization of HVGO by  $\text{CoNiMoS/Al}_2\text{O}_3$  and 15%  $\text{CoNiMoS/CeO}_2\text{-Al}_2\text{O}_3$  at Pressure: 40 bar, LHSV:  $1\text{ h}^{-1}$ ,  $\text{H}_2$ / Feed: 300:300 L/L.**

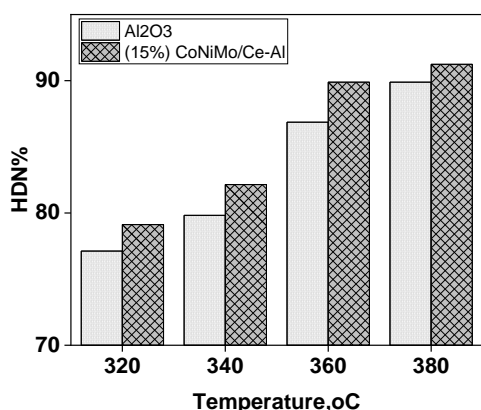


**Fig. 4b: Effect of reaction temperature on hydrogenation of HVGO by CoNiMoS/Al<sub>2</sub>O<sub>3</sub> and 15% CoNiMoS/CeO<sub>2</sub>-Al<sub>2</sub>O<sub>3</sub> at Pressure: 40 bar, LHSV: 1 h<sup>-1</sup>, H<sub>2</sub>/ Feed: 300:300 L/L.**

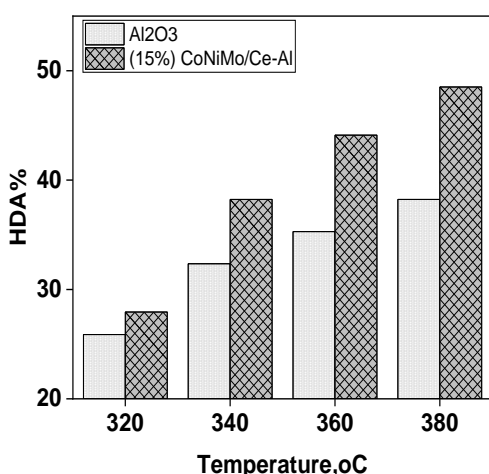


**Fig. 4c: Effect of reaction temperature on hydrodearomatization of HVGO by CoNiMoS/Al<sub>2</sub>O<sub>3</sub> and 15% CoNiMoS/CeO<sub>2</sub>-Al<sub>2</sub>O<sub>3</sub> at Pressure: 40 bar, LHSV: 1 h<sup>-1</sup>, H<sub>2</sub>/ Feed: 300:300 L/L.**

### 3.4.2 Effect of Reaction Pressure

In this step, the effect of applying different operating hydrogen pressures on the process of HT was studied while utilizing the picked optimum reaction temperature from prior section. Also, LHSV of 1 was employed during the current step of investigation. The impact of the pressure discrepancy on the values of HDS, HDN and HDA is illustrated in Figure 5.

The increment of hydrogen pressure inside the reactor could in turn enhance the rates of HDs, HDN and

HDA. This observation may be attributed to the raised amount of hydrogen as well as its partial pressure during the reaction by the pressure increase. These increments could consequently enhance the probability of interaction between hydrogen molecules and the hydrocarbon compounds of the HVGO [18]. Therefore, increased percentages of HDS, HDN and HDA could be achieved by the increase of pressure gradients. Nevertheless, the rates of increase in HDS, HDN and HDA percentages are dissimilar through the subsequent increases of equal pressure intervals.

In practical, significant increases in their values could be attained by the two catalysts by elevating the pressure from 20 to 40 bar. For instance, HDS values could be increased from 76 % and 53.36 (at low pressure) to 83.5 and 66.2 % (at higher pressure) by the composites containing 15% of ceria and pure alumina respectively. These values were then increased respectively to 86.9 and 78.23 % by the increase of pressure to 60 bar. Similar trend in the values of HDN and HDA, by the two composites, could be also noticed by the increase of pressure from 20 to 40 then to 60 bar. Based on the illustrated results, pressure of 40 bar has been chosen as the optimum value. This selection had been either of economic perspectives in terms of reducing the amount of utilized hydrogen gas during the HT process.

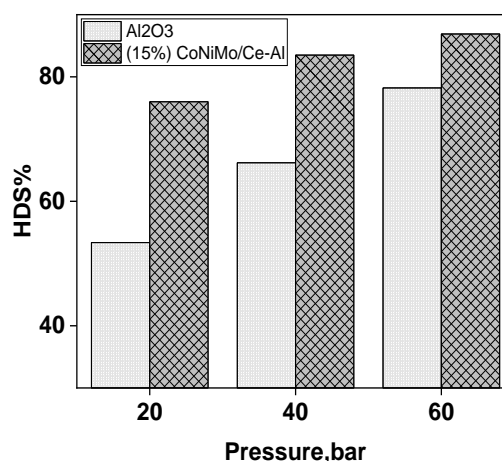


**Fig. 5a: Effect of reaction pressure on hydrodesulfurization of HVGO by CoNiMoS/Al<sub>2</sub>O<sub>3</sub> and 15% CoNiMoS/CeO<sub>2</sub>-Al<sub>2</sub>O<sub>3</sub> at Temperature: 360°C, LHSV: 1 h<sup>-1</sup>, H<sub>2</sub>/ Feed: 300:300 L/L.**

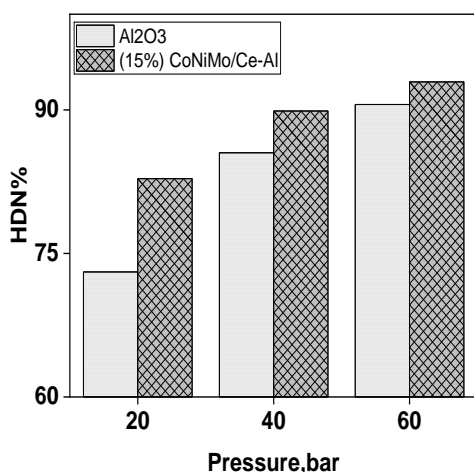


**Fig. 5b:** Effect of reaction pressure on hydrodenitrogenation of HVGO by CoNiMoS/Al<sub>2</sub>O<sub>3</sub> and 15% CoNiMoS/CeO<sub>2</sub>-Al<sub>2</sub>O<sub>3</sub> at Temperature: 360°C, LHSV: 1 h<sup>-1</sup>, H<sub>2</sub>/ Feed: 300:300 L/L.

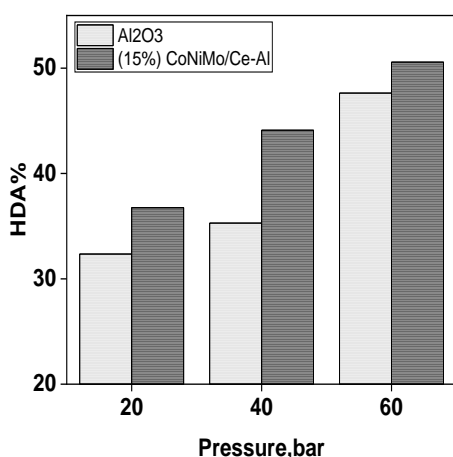


**Fig. 5c:** Effect of reaction pressure on hydrodearomatization of HVGO by CoNiMoS/Al<sub>2</sub>O<sub>3</sub> and 15% CoNiMoS/CeO<sub>2</sub>-Al<sub>2</sub>O<sub>3</sub> at Temperature: 360°C, LHSV: 1 h<sup>-1</sup>, H<sub>2</sub>/ Feed: 300:300 L/L.

### 3.4.3 Effect of Liquid Hour Space Velocity

In this step, the effect of LHSV change on the activity of the composites toward the HDS, HDN and HDA % was investigated. In the current step, the optimal reaction temperature and pressure that were acquired from the former two steps were employed. The impact of LHSV change on the rates of HDS, HDN and HDA of produced HVGO are shown via Figure 6.

In contrast to the inflation of both reaction temperature and pressure, the increase of LHSV could exhibit a turnaround attitude toward the HDS, HDN and HDA %. Specifically, the increment of the LHSV value had been inversely proportional with the values of HDS, HDN and HDA of the collected HVGO. In practical, the increase of LHSV value had been joined by increases in the contents of sulfur, nitrogen and aromatics compounds in the HVGO. Hence, limited percentages of HDS, HDN and HDA could be attained. This attitude can be explained by the rapid flow of HVGO molecules over the catalysts particles by increase of LHSV. Thus, little contact time between feedstock and catalysts: hence no proper interaction could take place [19]. In conclusion, it can be stated that the optimum value of LHSV is found to be 1 h<sup>-1</sup>.

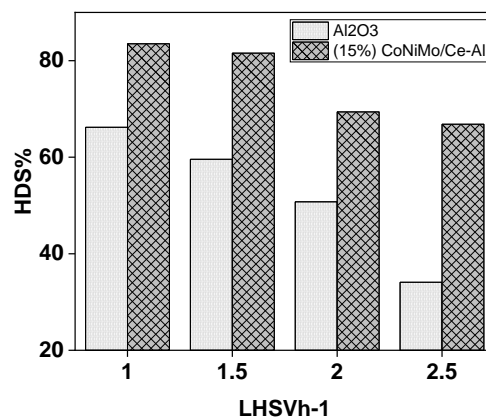


**Fig. 6a:** Effect of LHSV on hydrodesulfurization of HVGO by CoNiMoS/Al<sub>2</sub>O<sub>3</sub> and 15% CoNiMoS/CeO<sub>2</sub>-Al<sub>2</sub>O<sub>3</sub> at Temperature: 360°C, Pressure: 40 bar, H<sub>2</sub>/ Feed: 300:300 L/L.

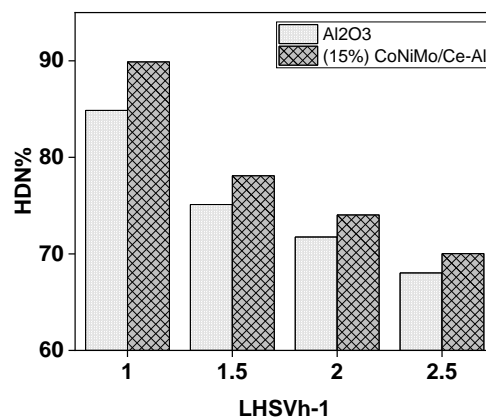


**Fig. 6b: Effect of LHSV on hydrodenitrogenation of HVGO by CoNiMoS/Al<sub>2</sub>O<sub>3</sub> and 15% CoNiMoS/CeO<sub>2</sub>-Al<sub>2</sub>O<sub>3</sub> at Temperature: 360°C, Pressure: 40 bar, H<sub>2</sub>/Feed: 300:300 L/L.**

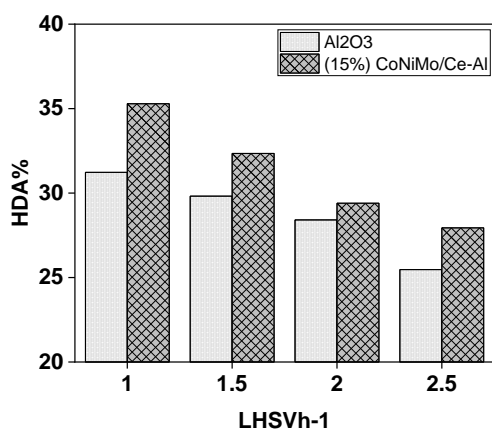


**Fig. 6c: Effect of LHSV on hydrodearomatization of HVGO by CoNiMoS/Al<sub>2</sub>O<sub>3</sub> and 15% CoNiMoS/CeO<sub>2</sub>-Al<sub>2</sub>O<sub>3</sub> at Temperature: 360°C, Pressure: 40 bar, H<sub>2</sub>/Feed: 300:300 L/L.**

## Conclusion

By completion of this study it can be concluded that the binary supported composites had generally showed better catalytic activity than that of the alumina supported composite. Its increased catalytic performance over the alumina supported one is referred to the combination between alumina and ceria in the composites. The incorporation of ceria within the structure of alumina could provide a phase separation between the particles of alumina and the metallic sites of the composites. This separation could lead to avoiding the formation of passive phases in this composite. Particularly, the presence of ceria could prevent the obtainment of metals aluminates which consequently may reduce the catalytic performance of this composite.

## References

- [1] J. Verstraete, K. Le Lannic and I. Guibard, Modeling fixed-bed residue hydrotreating processes, *Chemical engineering science* 62(18-20) (2007) 5402-5408.
- [2] D. Remesat, B. Young and W. Svrcek, Improving vacuum gas oil hydrotreating operation via a lumped parameter dynamic simulation modeling approach, *Chemical Engineering Research and Design* 87(2) (2009) 153-165.
- [3] A. Alvarez and J. Ancheyta, Modeling residue hydroprocessing in a multi-fixed-bed reactor system, *Applied Catalysis A: General* 351(2) (2008) 148-158.
- [4] R. Harding, A. Peters and J. Nee, New developments in FCC catalyst technology, *Applied Catalysis A: General* 221(1-2) (2001) 389-396.
- [5] W. N. W. Abdullah, R. Ali and W. A. W. A. Bakar, In depth investigation of Fe/MoO<sub>3</sub>-PO<sub>4</sub>/Al<sub>2</sub>O<sub>3</sub> catalytic oxidative desulfurization of Malaysian diesel with TBHP-DMF system, *Journal of the Taiwan Institute of Chemical Engineers* 58 (2016) 344-350.
- [6] R. Hamiye, C. Lancelot, P. Blanchard, J. Toufaily, T. Hamieh and C. Lamonier, Diesel HDS performance of alumina supported CoMoP catalysts modified by sulfone molecules produced by ODS process, *Fuel* 210 (2017) 666-673.
- [7] P. Sikarwar, U. A. Kumar, V. Gosu and V. Subbaramaiah, Catalytic oxidative desulfurization of DBT using green catalyst (Mo/MCM-41) derived from coal fly ash, *Journal of Environmental Chemical Engineering* 6(2) (2018) 1736-1744.
- [8] A. Stanislaus, A. Marafi and M. S. Rana, Recent advances in the science and technology of ultra low sulfur diesel (ULSD) production, *Catalysis today* 153(1-2) (2010) 1-68.
- [9] V. M. Gonzalez-DelaCruz, J. P. Holgado, R. Pereñíguez and A. Caballero, Morphology changes induced by strong metal-support interaction on a Ni-ceria catalytic system, *Journal of Catalysis* 257(2) (2008) 307-314.
- [10] N. Laosiripojana, W. Sutthisripok and S. Assabumrungrat, Synthesis gas production from dry reforming of methane over CeO<sub>2</sub> doped Ni/Al<sub>2</sub>O<sub>3</sub>: Influence of the doping ceria on the resistance toward carbon formation, *Chemical Engineering Journal* 112(1-3) (2005) 13-22.
- [11] S. Wang and G. M. Lu, Role of CeO<sub>2</sub> in Ni/CeO<sub>2</sub>-Al<sub>2</sub>O<sub>3</sub> catalysts for carbon dioxide reforming of methane, *Applied Catalysis B: Environmental* 19(3-4) (1998) 267-277.
- [12] M. Obulesu, *Parkinson's Disease Therapeutics: Emphasis on Nanotechnological Advances*, Academic Press 2020.

- [13] A. Trovarelli, Catalytic properties of ceria and CeO<sub>2</sub>-containing materials, *Catalysis Reviews* 38(4) (1996) 439-520.
- [14] A. Piras, A. Trovarelli and G. Dolcetti, Remarkable stabilization of transition alumina operated by ceria under reducing and redox conditions, *Applied Catalysis B: Environmental* 28(2) (2000) L77-L81.
- [15] Q. Zhuang, Y. Qin and L. Chang, Promoting effect of cerium oxide in supported nickel catalyst for hydrocarbon steam-reforming, *Applied catalysis* 70(1) (1991) 1-8.
- [16] N. Deraz, The comparative jurisprudence of catalysts preparation methods: I. Precipitation and impregnation methods, *J. Ind. Environ. Chem* 2(1) (2018) 19-21.
- [17] F. El Kady, M. Abd El Wahed, S. Shaban and A. A. El Naga, Hydrotreating of heavy gas oil using CoMo/ $\gamma$ -Al<sub>2</sub>O<sub>3</sub> catalyst prepared by equilibrium deposition filtration, *Fuel* 89(11) (2010) 3193-3206.
- [18] H. A. El Sayed, A. M. El Naggar, B. H. Heakal, N. E. Ahmed, S. Said and A. A. Abdel-Rahman, Deep catalytic desulphurization of heavy gas oil at mild operating conditions using self-functionalized nanoparticles as a novel catalyst, *Fuel* 209 (2017) 127-131.
- [19] A. M. El Naggar, M. S. Mostafa and M. T. Zaky, New trend for the pour point depression of a waxy petroleum fraction with in-situ desulphurization using (O<sub>2</sub>H & OH) radicals coupled with nanoparticles of titanium compounds, *Fuel* 180 (2016) 218-227.